A Wall Imperfection Channel Model for Signal Level Prediction and its Impact on Smart Antenna Systems for Indoor Infrastructure WLAN

Karim Medhat Nasr, *Member, IEEE*, Fumie Costen, and Stephen K. Barton, *Senior Member, IEEE*

***Abstract*—This paper presents a novel approach for the estimation of the local average signal level in an indoor environment based on a wall imperfection model. A ray-tracing tool based on the method of images with angular information, is first used to estimate the distribution of field strength (or coverage) in an arbitrary environment. The concept of spatial sampling is highlighted. The wall imperfection model is then introduced to study the sensitivity of the received signal level at an arbitrary location to imperfect wall positioning and electromagnetic material properties. An alternative approach to estimate the local mean signal level at a particular point is presented based on the wall imperfection model to reduce the computation time. The impact of the wall imperfection model on the patterns of a smart antenna system serving multiple users in an infrastructure WLAN is studied.**

***Index Terms*—Smart antennas, space division multiple access (SDMA), spatial indoor channel modeling, wall imperfections, WLAN.**

I. Introduction

THE flexibility and ease of deployment offered by WLAN standards such as IEEE801.11a and HIPERLAN 2 [1], [2] make them an attractive solution for many applications. One of the possible applications is wired LAN replacement [3], [4]. Smart antennas and space division multiple access (SDMA) [5]–[7] can increase the capacity of the wireless LAN. Spatial channel models capable of predicting the angular behavior at both ends of the link are necessary to study smart antennas [8]–[10]. The main advantage of such models is the quick assessment of various scenarios through simulation without the need for a time-consuming measurement campaign and independent of any specific antenna array properties. This paper presents an approach to estimating the local mean signal level based on a wall imperfection model. The focus of the paper is the wall imperfection model presented as an acceleration technique to estimate the mean signal level compared to the spatial averaging technique using ray tracing. The accuracy of the ray tracing tool itself is not considered and the presented methodology for estimating the local mean signal level could be applied to any other ray tracer.

The paper is organized as follows: Section II presents the output of a ray-tracing tool [4] based on the method of images and capable of estimating the spatial channel impulse response by evaluating the direction of departure (DOD) and the direction of arrival (DOA) of the rays in any arbitrary architecture and positioning of both the transmitter and the receiver. The tool accounts for the line of sight (LOS), single and double reflections, diffraction from corners and transmission loss through objects. The main channel parameters of interest, namely: the mean excess delay, the delay spread, the coherence bandwidth, the Rice "k" factor and the angular spread at both the transmitter and the receiver are also evaluated. Section III extends the tool to calculate the relative signal level distribution in an arbitrary environment. The effect of spatial sampling on the obtained coverage contours is discussed. In Section IV, the sensitivity of the obtained signal level at a particular point to the imperfections of wall positions and their electromagnetic material properties is studied through a proposed wall imperfection model. A discussion of the model parameters, including the maximum wall displacement versus the angle of incidence and the number of computer runs, is presented. An alternative approach for the estimation of the signal level at a receiving point is introduced based on the wall imperfection model. The results of the mean signal level obtained from this model are compared with the spatial sampling approach for different cases. Section V discusses the impact of the uncertainty of the wall positions on the patterns of a smart antenna system serving multiple users in an infrastructure WLAN. Finally, Section VI concludes the paper.

Manuscript received October 15, 2004; revised June 22, 2005.

The authors are with the School of Computer Science, University of Manchester, M13 9PL Manchester, U.K. (e-mail: nasrk@cs.man.ac.uk; f.costen@cs.man.ac.uk; s.k.barton@cs.man.ac.uk).

Digital Object Identifier 10.1109/TAP.2005.858593

II. Channel Model and Parameters

Ray tracing is argued to be one of the most suitable methods to model an indoor environment based on site-specific information because of its accuracy [18]–[22]. The method of images considers all objects as potential reflectors and calculates the location of transmitter images. Ray paths are formed based on the location of the receiver, the transmitter and its associated images. Ray tracing based on images allows the exact calculation of the ray paths between given transmitter and receiver positions. Although ray tracing is computationally complex and demanding, it has the inherent possibility to estimate the angular information [11] used for smart antennas investigations. The method of images is favored compared to ray launching, which can suffer from resolution problems and double counting of single ray paths [18]. Ray launching is sometimes more computationally efficient if the number of objects considered is large. A ray-tracing tool based on the method of images [4] is used for the case studies presented in this paper. The properties of

materials at 5.8 GHz [12], [13] are used to calculate the reflection and transmission coefficients for a TEM wave with perpendicular polarization for common building materials. The ray-tracing tool accounts for the LOS, single and double reflections, diffraction from corners and transmission loss through objects. In [24], it was shown that a ray tracer accounting only for double reflections gives delay spread results within 5% of the accurate measured figure at 60 GHz. In this paper, the main concern is a computationally efficient and an acceleration technique for estimating local mean signal levels hence double reflections are sufficient for showing this purpose.

The main radio channel parameters that can be approximately evaluated from the channel impulse response are the mean excess delay, the rms delay spread, the coherence bandwidth, the angular spread and the Rice "k" factor [14], [15], [27]. The ray tracing model used in the simulations assumes that most of the received power is contained in the strongest few paths mainly from large reflecting surfaces as noticed through measurements over a large band of frequencies. Indoor multipath measurements over a large range of frequencies (1.5 and 60 GHz) [23], [24] show that the power delay profile consists of a number of dominant echoes from large flat areas such as walls where most of the energy is confined interspersed with noise like clutter from smaller objects such as furniture and people across the entire range of delays. Correlated rays can add coherently as reported in [22]. The Rice k factor [27] is generally defined as the ratio between the power of the coherent or dominant component(s) to the power of the non coherent or scattered components. An approximate k factor is calculated in the context of the presented deterministic ray tracing tool as a "LOS power factor" or the power of the LOS ray divided by the power of the multipath rays and gives an indication of the obstruction of the LOS path.

There are many approaches to calculate the coherence bandwidth. One of the most accurate ways in calculating the coherence bandwidth is using the measured or simulated frequency autocorrelation function. A number of relationships have been reported in [14], [15], [25], [26]. The coherence bandwidth is defined as the bandwidth over which the frequency autocorrelation function is above a certain level (0.9 or 0.5). If the definition is relaxed so that the frequency autocorrelation function is above 0.5, then an approximate coherence bandwidth can be calculated as one fifth the inverse of the rms delay spread [14], [15]. The rms delay spread is the second central moment of the power delay profile [14], [15]. In analogy to the rms delay spread calculation, angular spread values at both sides of the link can be calculated as the second central moment of the power angle profile.

An arbitrary indoor environment is investigated (Fig. 1). A LOS path exists between the transmitter and the receiver. The LOS distance between the transmitter and the receiver is nearly 5 m. The channel impulse response results are shown in Fig. 1, the power-delay-angle profile (PDAP) in Fig. 2 and approximate values for the channel parameters are summarized in Table I.

Although the mean excess delay, the delay spread, the coherence bandwidth and the k factor can be predicted in advance (since a small unobstructed environment will generally have a small delay spread, a large coherence bandwidth, a k factor

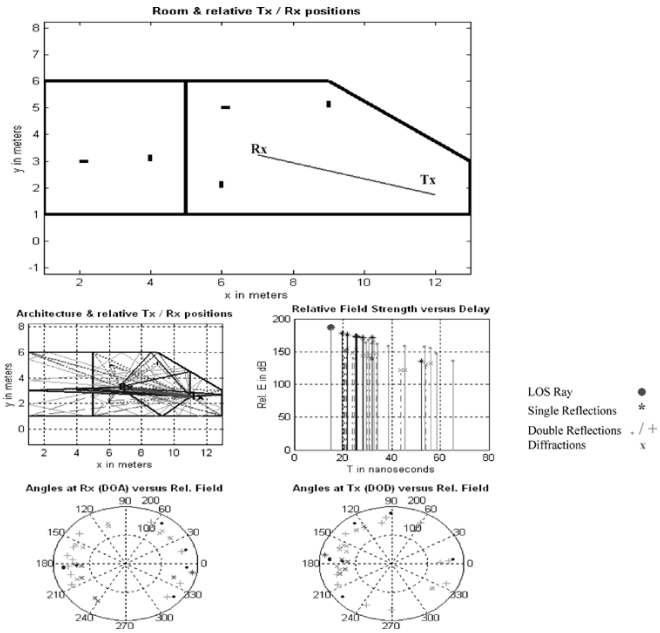

Fig. 1. Studied architecture and spatial channel impulse response.

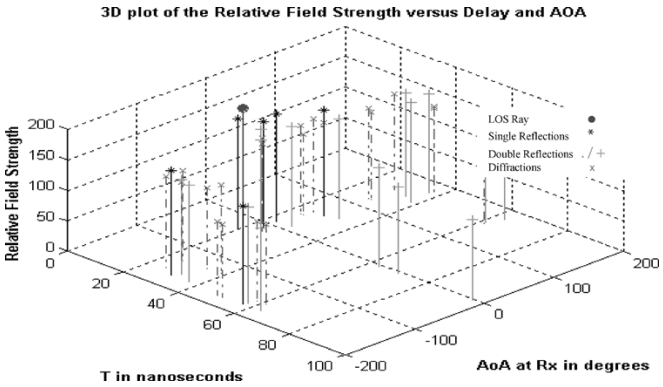

Fig. 2. PPDAP.

TABLE I
APPROXIMATE STATISTICAL CHANNEL PARAMETERS FOR THE STUDIED SCENARIO OF FIG. 1

Parameter	Value
Mean Excess Delay (ns)	19.11
rms Delay Spread (ns)	3.49
Approximate Coherence Bandwidth (MHz)	57.30
"K" Factor	2.11(3.2dB)
DOA Angular Spread (Degrees)	32.19
DOD Angular Spread (Degrees)	24.60

greater than 1 while a large obstructed environment will generally have a large delay spread, a small coherence bandwidth and a k factor less than 1), the angular parameters depend on the exact positions of both the transmitter and the receiver and on the architecture involved and do not follow a general rule.

III. SIGNAL LEVEL DISTRIBUTION PREDICTION AND SPATIAL SAMPLING

Contour plots of signal level distribution (coverage diagrams) can be used for the purpose of network planning and the deployment of access points (AP) in a WLAN. The various rays, having travelled over paths of different lengths are added at the

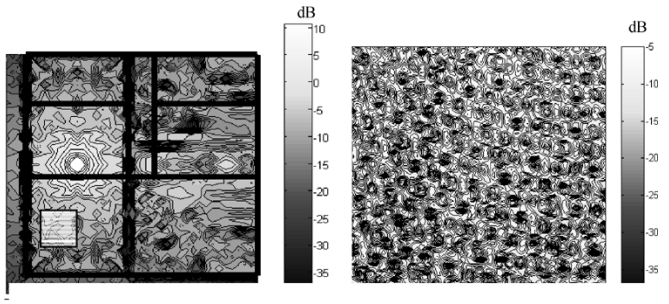

(a) 25cm grid:(40x40)points (b)1.25 cm grid: (80 x 80)points

Fig. 3. Contour plots for the relative signal strength in dB for a 10 m × 10 m indoor environment (a) and (b) details of shadowed block of (1 m × 1 m) at position (2,2)m.

receiver to produce the characteristic Rice distributed multipath fading (or as a special case Rayleigh when the LOS path is obstructed). Nyquist spatial sampling theorem requires sampling at intervals of "at most" $\lambda/2$ to avoid aliasing. In this paper, to guarantee spatial anti-aliasing and improve the accuracy of signal level prediction, the spatial sampling points are separated by $\lambda/4$ intervals. For coverage purposes, the interest is in the local mean signal level, averaging out the effects of fading.

The sampling interval or the separation between sampling points is taken as 1.25 cm which is approximately $\lambda/4$ at 5.8 GHz. Averaging over a block of $10\lambda \times 10\lambda$ (50 cm × 50 cm) square requires a large number ($40 \times 40 = 1600$) of points separated by $\lambda/4$ to be calculated for averaging. Subsampling (i.e., using grids with points separated more than $\lambda/4$ or 50 or 25 cm intervals instead of 1.25 cm) will not produce a true coverage plot as each sample is still subject to fading. This effect is referred to as spatial aliasing. Fig. 3(a) shows a contour plot of signal strength over a 10 m × 10 m floor plan based on sub sampling at 25 cm ($\sim 5\lambda$) intervals and the phasor addition of all the rays forming the PDAP profile at every point of the grid. With a 25 cm grid in the 10 m × 10 m architecture, 1600 points are required. This is contrasted to using a grid of points with 1.25 cm which would require 640 000 points. Fig. 3(b) shows an expanded view of a (1 m × 1 m) section sampled at 1.25 cm ($\lambda/4$) intervals. Clearly a small offset in the sampling points of Fig. 3(a) would have made a large difference to the values sampled. However, the computation time increases linearly with the number of points sampled, so an increase in resolution from 5λ to $\lambda/4$ increases the computation time 400-fold.

The simulation results of Fig. 3 agree with the expected behavior described above and with [16] confirming that the multipath behavior inside buildings exhibits strong variations as either the transmitting or the receiving antenna is moved over a distance of the order of $\lambda/2$.

For network planning purposes, the interest is to estimate the expected local mean level. Averaging large blocks ($10\lambda \times 10\lambda$) of 1600 points separated by $\lambda/4$ to estimate the local mean level requires enormous computational resources. An alternative approach to estimating the expected local mean level, based on artificially modulating the wall surfaces to cover all the possible signal phases will be described in the next section. This model can also be used to study the effect of the imperfections in the wall positions and material properties and its impact on smart antenna systems, as will be shown in Section V.

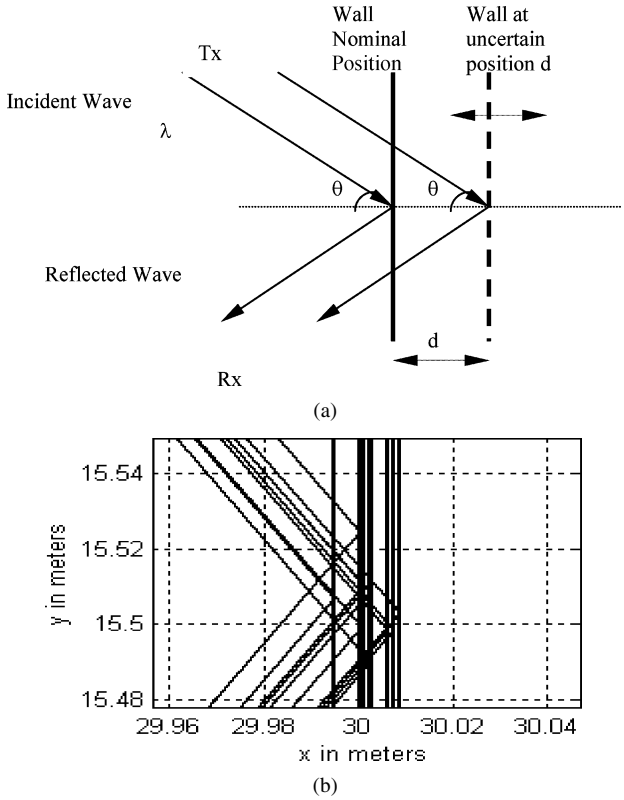

Fig. 4. (a) Reflection from a single wall used to derive the angle of incidence/wall distance relationship. (b) Application of the model to a single wall showing the multiple positions and the levels of single reflections at an incidence angle of 55° and 10 computer runs.

IV. Modelling of Wall Imperfections

A. Development of the Model

In all the above simulation cases, the walls (or objects) were assumed to be perfectly flat. In a more realistic situation, the positions of the walls as well as the accuracy of the values of the electromagnetic wall properties used in the model can affect the predicted signal strength. It is interesting to study the sensitivity of the obtained phasor sum of the rays to such imperfections.

The proposed model to study the sensitivity to wall positions is implemented by randomly varying the position of each wall using a uniformly distributed random variable over a number of computer runs. The uniform distribution is selected to calculate the local mean field strength by averaging out all phases with equal weighting. A similar methodology can be used to study imperfections of wall material properties by adding a random variable with an arbitrary distribution (uniform or Gaussian) to the electromagnetic wall property values to account for uncertainties in these values.

The standard deviation of the random variable can be varied to study different degrees of wall displacement. A similar approach is used to study the uncertainties in the nominal values of electromagnetic properties (dielectric constant and conductivity) of the building materials used in the scenario. The standard deviation of the random variable is chosen such that the phase of the obtained relative electric field spans the whole range of all possible angles (i.e., 2π). The phasor sum of the LOS ray between a transmitter and a receiver and the reflected ray from a single wall are considered [Fig. 4(a) and (b)]. Two maximum wall

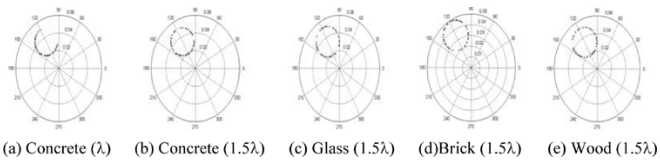

Fig. 5. Polar plot of the received level showing (a) an incomplete circle of electric field phases for a concrete wall with a maximum wall displacement of λ and (b) a complete circle of phases for a maximum displacement of 1.5λ and 50 runs for concrete, (c) glass, (d) brick, and (e) wood as examples of different materials.

displacement of λ and 1.5λ in Fig. 5(a) and (b) show the loci of the resultant phasor (obtained by adding the contribution of the LOS ray and the single reflection) for a concrete wall. The formation of the partial and the full electric field phase circles is shown. The formation of the full phase circle clearly depends on the angle of incidence to the wall and the number of computer runs. Different materials with different electromagnetic properties (dielectric constant and conductivity) were also simulated. The type of material does not affect the formation of the full phase circle. Simulation results showed that the impact of uncertainties in the material properties can be ignored when considering the formation of the full phase circle [e.g, Fig. 5(b)–(e)]. The local mean field strength at the receiver is then calculated by averaging all the values of the full phase circle. This proposed approach in estimating the average local value of the signal strength, has the advantage of decreasing the number of computer runs compared to the approach of averaging blocks of points with high resolution ($\lambda/4$) grids.

The relationship linking the angle of incidence, the minimum wall distance to achieve a phase shift of 2π and the wavelength can be obtained by considering a single plane wave impinging on the wall as shown in Fig. 4(a).

It can be easily observed that the path difference (p) between the two reflected rays is given by

$$p = 2d\cos\theta. \tag{1}$$

The phase difference (ϕ) is obtained by multiplying the path difference by the propagation constant ($k = 2\pi/\lambda$)

$$\phi = \left(\frac{2\pi}{\lambda}\right) \cdot (2d\cos\theta). \tag{2}$$

For a whole phase rotation (i.e., $\phi = 2\pi$) then

$$d = \frac{\lambda}{(2\cos\theta)}. \tag{3}$$

Equation (3) shows that the wall displacement is linked to the angle of incidence through a $(1/\text{cosine})$ relationship. In order to verify this theory and to determine the minimum displacement of the wall position, the minimum number of computer runs to cover all the range of phases, a single wall scenario is simulated for different angles of incidence and the polar plot of the field strength is monitored to check whether the full range of phases is covered. The relationship between the minimum necessary wall displacement normalized to the wavelength versus the angle of incidence and the minimum number of computer runs is shown in Fig. 6 both for simulation and theory [(3)]. A

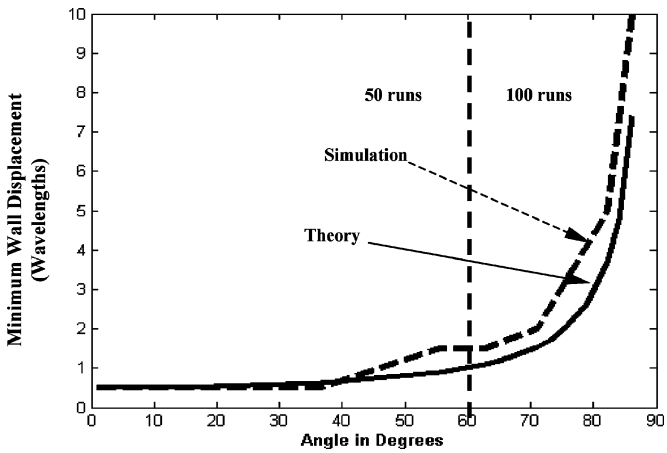

Fig. 6. Relationship between the minimum wall displacement in wavelengths, computer runs and the angle of incidence in degrees (theory versus simulation).

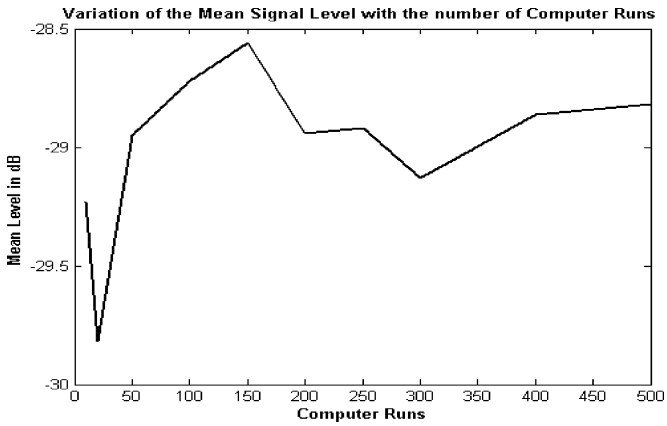

Fig. 7. Effect of the number of computer runs on the stabilization of the mean signal level.

good agreement between the theory and simulation is observed. The necessary wall displacement should be at least $\lambda/2$ for angles of incidence less than 40° and starts to increase, following a $(1/\text{cosine})$ curve, reaching $\sim 10\lambda$ for angles of incidence of approximately 85°. In a multiple wall scenario, the movements of the walls need to be uncorrelated, hence the use of the random distribution. The number of computer runs impacts the formation of the full phase circle and more than 100 runs are normally necessary for angles above 70°. Increasing the number of computer runs and averaging the signal level over more points, result in the stabilization or convergence of the estimated local mean level. Simulation results show that nearly 300 runs are enough to achieve less than 0.3 dB variation in the estimated local mean level when a single wall is considered (Fig. 7).

B. Application Case Studies

The wall imperfection model described above was tested for several architectures and several positions within each architecture. The model is first applied to estimate the mean signal level at a receiving point (15,15)m in an arbitrary indoor environment of 30 m × 30 m (Fig. 8). The procedure is described as follows. The scenario is first simulated using the original ray-tracing tool to determine the largest incidence angle of the rays impinging on each wall. Fig. 6 is then used to determine the minimum required

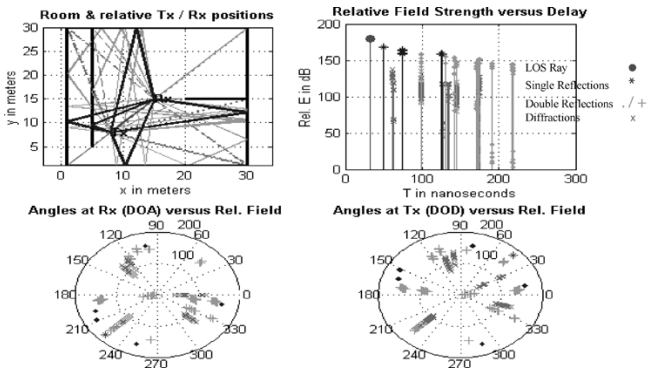

Fig. 8. Application of the imperfection model to an arbitrary scenario with 50 runs.

movement for each wall to cover all possible phases. An optional additional random variable with a 10% standard deviation (selected arbitrarily) is added to the values of the electromagnetic properties of the walls (permittivity and conductivity) to account for uncertainties in these values. During each computer run, all the walls are moved simultaneously and randomly to give uncorrelated wall movements and the phasor sum of all the rays arriving at the receiver is obtained . The values of n computer runs are then averaged to obtain an estimate of the local mean field strength at the receiving point. The estimated level is compared with the value obtained by averaging a block of points around the receiver separated by less than $\lambda/4$ without any imperfection as was shown in Section III. The obtained averaged field value is compared for different computer runs (for the wall imperfection model) and different number of points forming the averaging block (for the spatial sampling approach). The results are summarized in Table II. The results from averaging blocks of points following the spatial sampling approach suggest that averaging 400 points ($5\lambda \times 5\lambda$) seems to be enough for indoor environments to reach a stable average value after minimizing the effect of small signal variations. This is contrasted to the traditional approach used in outdoor environments [16] of averaging larger blocks of ($10\lambda \times 10\lambda$) or ($20\lambda \times 20\lambda$). The average field level obtained from the wall imperfection model seems to have reached its final value after 50 to 100 runs. The average value for 50 runs for the wall imperfection model is -19.39 dB compared to an average value of -19.32 dB for the spatial sampling approach with 400 points showing a 0.07 dB difference in the estimated signal value with a reduction of 87.5% in the number of computer runs. Fig. 9 shows the simulation results for the spatial sampling approach with 6400 points and the wall imperfection model with 300 computer runs.

The wall imperfection model was tested and compared to the spatial sampling approach at several locations [Fig. 10(a)] (obstructed and unobstructed) inside the architecture of Fig. 8. The average difference between the mean field value of the wall imperfection model with 50 runs and the mean values with 400 points of the spatial sampling approach (averaged over all locations) is less than 0.7 dB showing the consistency of the model. The results are summarized in Fig. 10(b). The model was also tested in different arbitrary architectures with different number of walls and at several positions. Good agreement between the value achieved from the wall imperfection model and the spatial sampling approach is found. A comparison of the two models at arbitrary points inside different architectures is summarized in Fig. 10(c). The difference between the mean value estimated from both models averaged over all the tested architectures and points is again less than 0.7 dB showing its consistency.

This section developed the wall imperfection model and proposed a new approach for average signal level prediction in an arbitrary indoor environment. A comparison between the spatial sampling approach and the wall imperfection model showed that it is possible to predict the average signal level with adequate accuracy using the wall imperfection model with the advantage of a reduction of over 85% in the number of computer runs. The next section will study the impact of small movements in the position of users, AP and walls on the performance of a smart antenna system in an indoor WLAN.

V. A Comparison of User/AP Movement Versus the Wall Imperfection Model and its Impact on Smart Antenna Systems for WLAN

In this section, the impact of moving the position of a WLAN AP or the user by less than a wavelength on the performance of a smart antenna system is assessed and compared with the variation of the position of the walls using the wall imperfection model. A smart antenna system serving multiple users through SDMA in an indoor infrastructure WLAN was studied in detail in [4], [17]. In [17], it is assumed that the channel characteristics are perfectly known at the AP and this information is used to adapt the weights of a smart antenna to serve multiple users simultaneously. It is expected that small user, AP or wall displacements ($\sim \lambda/4$) will cause a variation of the smart antenna patterns and consequently the Signal to Interference plus Noise Ratio (SINR) in the multipath case due to the change of the phase and amplitude of the multipath components (rays) arriving at the AP. A simulation case study is presented to illustrate the above. In Fig. 11, four users are served simultaneously by an AP in an SDMA scheme. A uniform linear array (ULA) smart antenna is deployed at the AP with four antenna elements. The smart antenna algorithm relies on Sample Matrix Inversion (SMI) and trades off interference and noise following a minimum mean square Error (MMSE) criterion [5], [6], [17].

For high signal to noise ratio (SNR) per antenna element (above 20 dB), the array will operate in the zero forcing region completely eliminating interference by adjusting the phasor contributions of the rays in favor of the intended user. For low SNR (below 10 dB), the array will operate in the "beamsteering" region [17] acting as a spatial matched filter to mitigate the effect of noise. We consider here an SNR of 60 dB per antenna element as an example, hence a zero forcing behavior (the same behavior is noticed for SNRs as low as 20 dB). The corresponding normalized antenna patterns for the four users with perfect channel estimation are shown in Fig. 12(a) when the LOS ray only is considered and Fig. 12(b) when the multipath rays are considered. The obtained SINR values for the four users are shown in Table III. The zero forcing behavior can be explained by observing the LOS case: Considering a specific user, the array places nulls in the patterns of each user in the direction of the other users while focussing the peak of

TABLE II
COMPARISON OF THE AVERAGE LOCAL FIELD VALUE AROUND THE RECEIVER OBTAINED FROM THE WALL IMPERFECTION MODEL AND THE SPATIAL SAMPLING APPROACH FOR DIFFERENT COMPUTER RUNS. (A) WALL IMPERFECTION MODEL (B) SPATIAL SAMPLING APPROACH

(a) Wall Imperfection Model		(b) Spatial Sampling Approach	
Number of Computer Runs	Average Field Value in dB	Number of Runs (Points separated by $\lambda/4$)	Average Field Value in dB
10	-18.92	100 ~ (2.5λ x 2.5λ)	-20.52
50	-19.39	400 ~ (5λ x 5λ)	-19.32
100	-19.34	1600 ~ (10λ x 10λ)	-19.30
200	-19.22	6400 ~ (20λ x 20λ)	-19.34
300	-19.45		

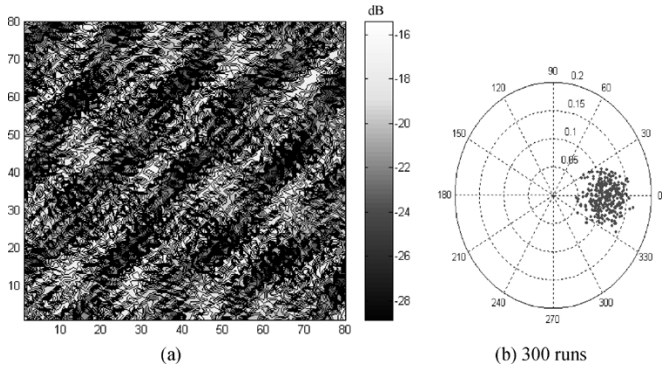

Fig. 9. (a) A block of 6400 points separated 1.25 cm ($\sim \lambda/4$) apart around the receiving point of Fig. 8(b) polar plot of the spreading of relative complex field values at the receiver with 300 runs of the wall imperfection model.

the pattern as near as possible in the direction of the intended user. In the special case of LOS the zero forcing algorithm results in null steering patterns. The SINR values can be larger than the SNR value since the array of four elements can achieve a maximum gain of 6.03 dB.

A. Impact of a Small Displacement in a User Position or the AP Position

User 1 at the original position of approx (11,23)m is moved by a fraction of a wavelength (less than 2 cms). It is expected that such a small movement would lead to a large variation in the shape of the multipath patterns due to the phasor contribution of the rays. This is contrasted to the LOS situation where very small variations can be observed. This is illustrated in Fig. 13. Comparing Figs. 12 and 13, it is noticed that very small changes occur in the patterns for the LOS case after the variation of User 1 position. The multipath patterns of Fig. 13 are totally different. A similar behavior is expected for a small displacement in the AP position. This is illustrated in Fig. 14.

The small variation in the position of one user or the AP leads also to a small variation in the SINR value as shown in Table III if the smart antenna system is quick enough to adapt to the new change. It is important that the smart antenna adapts quickly to these small changes in the position otherwise, a large degradation in the performance can occur. If the original patterns of Fig. 12 are used instead of the newly adapted patterns of Fig. 13 or Fig. 14 after the small variation of User 1 or the AP position, a severe degradation in the SINR occurs as illustrated in Table IV.

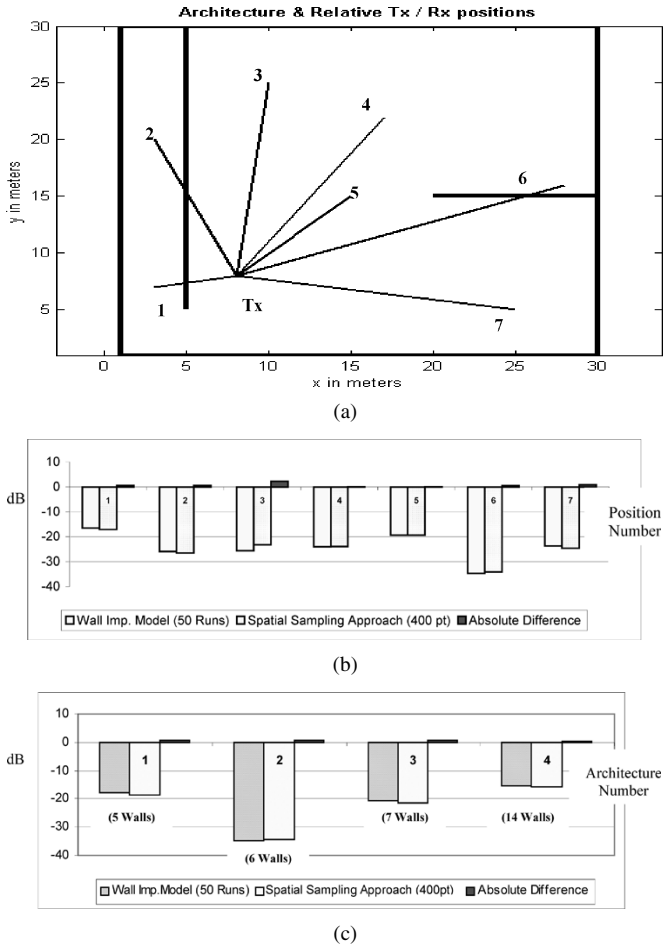

Fig. 10. (a) Testing positions inside the simulated scenario. (b) Comparison of the two models at the positions of Fig. 10(a). (c) Comparison of both models at positions in different architectures.

B. Impact of Wall Displacements

The wall imperfection model is then applied for different maximum wall displacements and the variation of the antenna patterns and SINR values are monitored. It is expected that, for the multipath case, as the maximum deviations of the walls increase more changes in the patterns and the SINR values will be observed compared with the LOS case.

The LOS case is not affected since only one ray is considered and its DOA is not affected by the variation of the wall positions. This is shown in Table V where the average SINR deviation (averaged over 20 runs i.e., 20 random wall displacements) for User 1 of Fig. 11 is monitored for a maximum wall displacement of 5 cm ($\sim \lambda$), 2.5 cm ($\sim \lambda/2$) and 1.25 cm ($\sim \lambda/4$). The average

TABLE III
SINR VALUES BEFORE AND AFTER A SMALL VARIATION OF USER 1 POSITION AND THE AP POSITION

	Original AP and Users Positions		New User 1 Position		New AP Position	
SINR (dB)	LOS	Multipath	LOS	Multipath	LOS	Multipath
User 1	65.15	60.78	65.10	59.99	65.42	58.90
User 2	65.21	56.71	65.30	56.30	65.53	58.54
User 3	65.25	61.03	65.33	61.51	65.52	62.65
User 4	65.42	57.84	65.26	56.96	65.68	56.19

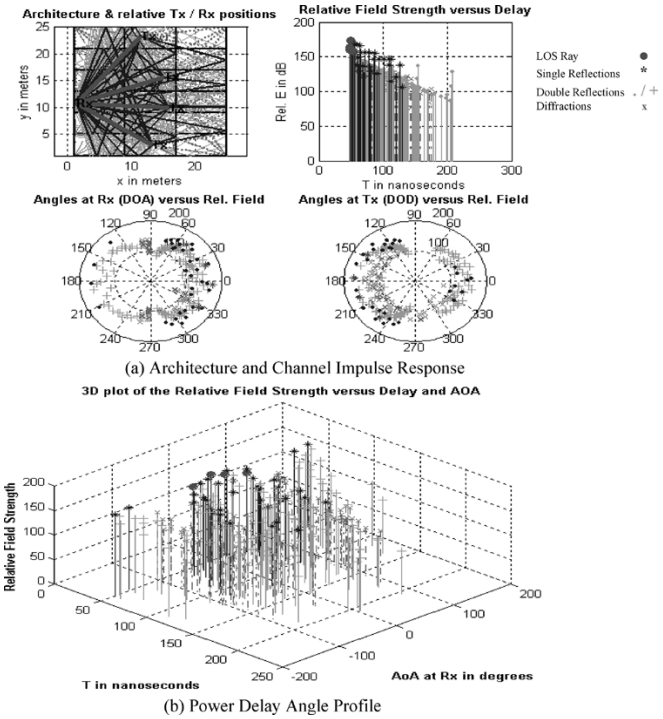

Fig. 11. Architecture of the SDMA scheme with four users and their corresponding PDAP.

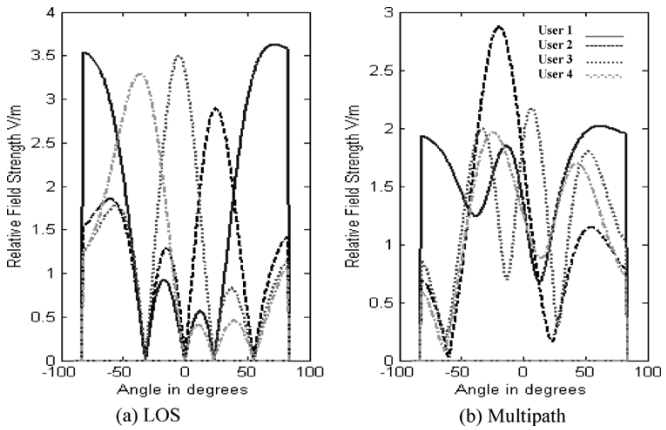

Fig. 12. Zero forcing patterns of the smart antenna system for the scenario of Fig. 11.

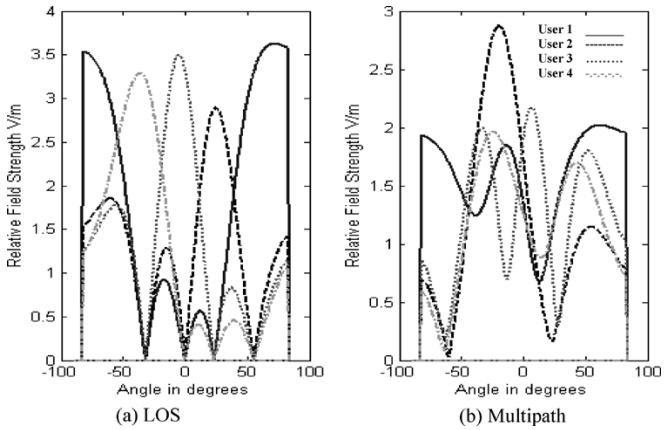

Fig. 13. Zero forcing patterns of the smart antenna system after changing the position of User 1 by a fraction of a wavelength.

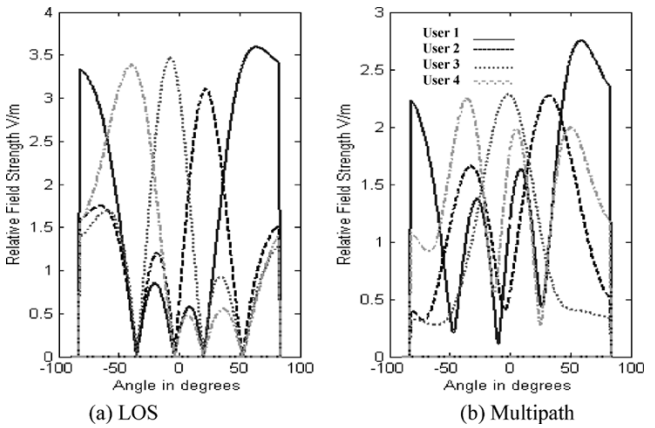

Fig. 14. Zero forcing patterns of the smart antenna system after changing the position of the AP by a fraction of a wavelength.

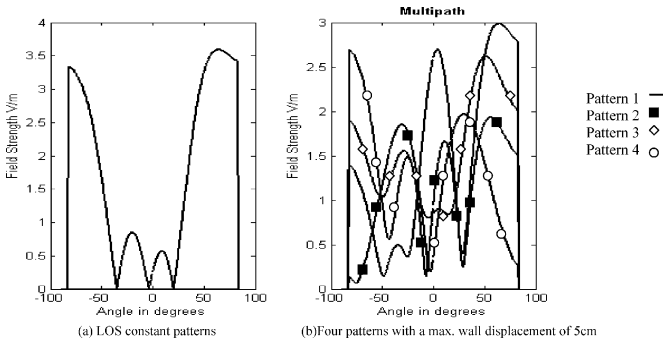

Fig. 15. Application of the wall imperfection model to User 1 of Fig. 11.

deviation of SINR values increases by roughly 2.5 dB each time the maximum wall displacement is doubled. Fig. 15(b) shows the large variation of the patterns of User 1 for a maximum deviation of ($5\ \mathrm{cm} \sim \lambda$) over four computer runs. This is contrasted with the constant patterns for the LOS case in Fig. 15(a).

The above simulation results show that small wall displacements (fractions of wavelength) would result in a totally different smart pattern in the multipath case and a deviation in the

TABLE IV
SINR VALUES KEEPING THE ORIGINAL PATTERNS AFTER THE VARIATION OF USER 1 POSITION AND THE AP POSITION

	New User 1 Position keeping original weights		New AP position keeping original weights	
SINR (dB)	LOS	Multipath	LOS	Multipath
User 1	65.01	58.79	26.34	3.43
User 2	29.82	2.16	21.21	-6.26
User 3	35.03	2.99	20.99	10.02
User 4	37.59	-1.85	29.36	-4.06

TABLE V
AVERAGE SINR DEVIATION FOR USER 1 FOR DIFFERENT MAXIMUM WALL DISPLACEMENTS OVER 20 RUNS

Displacement	Average SINR deviation
5 cm (~λ)	8.2 dB
2.5 cm (~λ/2)	5.6 dB
1.25 cm (~λ/4)	3.1dB

average SINR value increasing with the increase of the wall displacement. This case may be interesting from a system design perspective. A system designer should expect nominal SINR values to be achieved with some deviation based on the accuracy of the architectural layouts used for ray tracing compared to real life situations where main features positions like walls may have an error of few centimeters.

VI. CONCLUSION

In this paper, a wall imperfection model was presented and used to estimate the local mean signal level at the receiving point with computation efficiency. A ray-tracing tool was first used to estimate the power delay profile and the angular behavior at both sides of the wireless link. Contour plots with different resolutions were presented and the importance of adhering to a grid of points less than a half of a wavelength apart to avoid spatial aliasing to predict the fading behavior was highlighted. This however requires large computational resources.

The wall imperfection model can be used to study the sensitivity of the received signal level to wall position and material imperfections. The estimation of the local mean signal level is done by artificially modulating the positions of the walls to cover all possible signal phases and simulate the fading behavior. The parameters of the model include the maximum wall displacement, which depends on the angle of incidence and the number of computer runs to cover all the possible phases that would occur in an indoor fading environment. The model was tested through several case studies of arbitrary indoor architectures obstructed and unobstructed and with different number of walls. The wall imperfection model achieves more than 85% reduction in the number of computer runs compared to the spatial sampling grid approach showing its potential. The impact of small User or AP displacement on the performance of a smart antenna system was assessed. It was shown that if the smart antenna array does not adapt quickly to these small changes (fractions of a wavelength), a severe degradation of SINR value would be expected. The wall imperfection model was also used to assess the effect of different levels of wall displacements on the variation of the SINR values and the patterns of a smart antenna system serving multiple users in an infrastructure Indoor WLAN through an SDMA scheme. It was shown that, in contrast to the traditional approach of focusing a beam toward an intended user, small variations ($\sim \lambda/4$ to λ) in the positions of the walls can cause large variations in the patterns which take into account the phasor contributions of the multipath components. A deviation of the nominal SINR value occurs in the multipath case which highlights again the importance of adapting quickly to any small changes in the environment.

REFERENCES

[1] *Part II: Wireless LAN Medium Access Control (MAC) and Physical Layer (PHY) Specifications: High Speed Physical Layer in the 5 GHz Band, IEEE*, IEEE Sandard 802.11a/D7.0-1999, 1999.

[2] "Broadband Radio Access Networks (BRAN); HIPERLAN Type 2: Physical (PHY) Layer," ETSI, ETSI TS 101 475, 2000.

[3] K. M. Nasr, F. Costen, and S. K. Barton, "An application of smart antenna systems for archiving networks in TV studios," in *Proc. 13th IEEE Int. Symp. Personal, Indoor and Mobile Radio Communications PIMRC2002*, Lisbon, Portugal, Sep. 2002, pp. 232–236.

[4] ——, "A spatial channel model and a beamformer for smart antennas in broadcasting studios," in *Proc. 12th Inst. Elect. Eng. ICAP2003*, vol. 2, Exeter, U.K., 2003, pp. 828–831.

[5] J. H. Winters, "Smart antennas for wireless systems," *IEEE Personal Commun.*, pp. 23–27, Feb. 1998.

[6] J. C. Liberti and T. S. Rappaport, *Smart Antennas for Wireless Communications: IS-95 and Third Generation CDMA Applications*. Englewood Cliffs, NJ: Prentice-Hall, 1999.

[7] L. C. Godara, "Applications of antenna arrays to mobile communications part I: Performance improvement, feasibility and system considerations," *Proc. IEEE*, vol. 85, no. 7, pp. 1031–1060, Jul. 1997.

[8] G. Foschini and M. Gans, "On limits of wireless communications in a fading environment when using multiple antennas," *Wireless Personal Commun.*, vol. 6, no. 3, pp. 311–335, Mar. 1998.

[9] M. Steinbauer, A. F. Molisch, and E. Bonek, "The double directional radio channel," *IEEE Antennas Propag. Mag.*, vol. 43, no. 4, pp. 51–63, Aug. 2001.

[10] R. Ertel, P. Cardieri, K. Sowerby, and T. S. Rappaport, "Overview of spatial channel models for antenna array communications systems," *IEEE Personal Commun.*, pp. 10–22, Feb. 1998.

[11] P. H. Lehne and M. Petersen, "An overview of smart antenna technology for mobile communications systems," *IEEE Commun. Surveys*, vol. 2, no. 4, 1999.

[12] I. Cuinas and M. G. Sanchez, "Measuring, modeling and characterizing of indoor radio channel at 5.8 GHz," *IEEE Trans. Veh. Technol.*, vol. 50, pp. 526–535, 2001.

[13] F. Villanese, N. E. Evans, and W. G. Scanlon, "Pedestrian-induced fading for indoor channels at 2.45, 5.7 and 62 GHz," in *Proc. IEEE Vehicular Technology Conf. VTC2000*, 2000, pp. 43–48.

[14] T. S. Rappaport, *Wireless Communications: Principles and Practice*, 2nd ed. Englewood Cliffs, NJ: Prentice-Hall, 2002.

[15] R. Vaughan and J. B. Andersen, *Channels, Propagation and Antennas for Mobile Communications*. London, U.K.: The Institution of Electrical Engineers, 2003.

[16] W. Honcharenko, H. L. Bertoni, J. L. Dailing, J. Qian, and H. D. Yee, "Mechanisms governing UHF propagation on single floors in modern office buildings," *IEEE Trans. Veh. Technol.*, vol. 41, pp. 496–504, Nov. 1992.

[17] K. M. Nasr, F. Costen, and S. K. Barton, "An optimum combiner for a smart antenna in an indoor infrastructure WLAN," in *Proc. IEEE Vehicular Technology Conf. (VTC2003/Fall)*, vol. 1, Orlando, FL, Oct. 2003, pp. 193–197.

[18] B. S. Lee, A. R. Nix, and J. P. McGeehan, "Indoor space-time propagation modeling using a ray launching technique," in *Proc. 11th Int. Conf. Antennas and Propagation ICAP2001*, Apr. 2001, pp. 279–283.
[19] J. W. McKown and R. L. Hamilton, "Ray tracing as a design tool for radio networks," *IEEE Network Mag.*, pp. 27–30, Nov. 1991.
[20] M. F. Catedra and J. Perez-Arriaga, *Cell Planning for Wireless Communications*. Norwood, MA: Artech House, 1999.
[21] R. Valenzuela, "A ray tracing approach to predicting indoor wireless transmission," in *Proc. IEEE Vehicular Technology Conf. VTC93*, 1993, pp. 214–218.
[22] R. P. Torres, S. Loredo, L. Valle, and M. Domingo, "An accurate and efficient method based on ray-tracing for the prediction of local flat-fading statistics in picocell radio channels," *IEEE J. Select. Areas Commun.*, vol. 19, pp. 170–178, Feb. 2001.
[23] A. M. Saleh and R. A. Valenzuela, "A statistical model for indoor multipath propagation," *IEEE J. Select. Areas Commun.*, vol. SAC-5, pp. 128–137, Feb. 1987.
[24] P. F. M. Smulders and J. J. G. Fernandes, "Wide-band simulations and measurements of MM-wave indoor radio channels," in *Proc. 5th IEEE Int. Symp. Personal, Indoor and Mobile Radio Communications PIMRC94*, vol. 2, 1994, pp. 501–504.
[25] R. J. C. Bultitude, "Estimating frequency correlation functions from propagation measurements on fading radio channels: A critical review," *IEEE J. Select. Areas Commun.*, vol. 20, pp. 1133–1143, Aug. 2002.
[26] A. Hammoudeh and D. Scammell, "Frequency domain characterization of indoor wireless LAN mobile radio channel employing frequency and polarization diversity in the 63.4 GHz-65.4 GHz band," *IEEE Trans. Veh. Technol.*, vol. 53, no. 4, pp. 1176–1189, Jul. 2004.
[27] H. Hashemi, "The indoor radio propagation channel," *Proc. IEEE*, vol. 81, pp. 943–968, Jul. 1993.

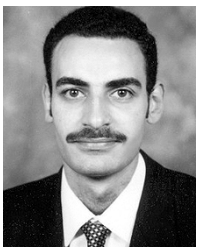

Karim Medhat Nasr (M'02) received the B.Sc. (Honors) and M.Sc. degrees in electronics and communication engineering from Cairo University, Giza, Egypt, in 1995 and 2000, respectively, and the Ph.D. degree from the University of Manchester, Manchester, U.K., in 2005. His M.Sc. thesis was on "Finite Difference Time Domain (FDTD) for Remote Sensing Applications" and Ph.D. thesis was on "Smart Antenna Systems for Indoor WLAN."

In 1996, he joined the Egyptian Radio and TV Union (ERTU) as a Project Engineer working on the design of digital broadcasting systems and electronic archiving networks. In September 2001, he was awarded an Overseas Scholarship and joined the Mobile Systems Architecture Group at the University of Manchester, Manchester, U.K. He is presently a Research Associate with the Mobile Systems Architecture Group at the University of Manchester, investigating a grant on Smart Antennas for WCDMA systems. During Spring 2005, he was a Visiting Researcher at the Antennas and Propagation Division of Aalborg University, Denmark, conducting indoor channel measurements and investigating propagation aspects for future MIMO and UWB systems through a European COST273 sponsored mission. He is a Reviewer for several transactions and international conferences. His current research interests include propagation modeling and computational electromagnetics, digital signal processing (DSP) for wireless systems, smart antennas and multiple element array processing multiuser MIMO systems, OFDM, and UWB.

Dr. Nasr is a Member of the Institution of Electrical Engineers (IEE), the IEE Manchester Branch Communication Broadcasting and Multimedia (CBM) Technical Group, the Wireless Home Networking Group, and European COST Action 273: "Toward Mobile Broadband Multimedia Networks."

Fumie Costen received the B.Sc. and M.Sc. degrees in electronics and the Ph.D. degree in informatics from Kyoto University, Kyoto, Japan, in 1991, 1993, and 2005, respectively.

She was involved in the design of a subsurface radar system to probe underground nondestructively, using monocycle pulse cylindrical wave. This research dealt with an inhomogeneous propagation medium and proposed an algorithm to estimate the indices of both the target and the medium and thus reconstruct the subterranean topography. In 1993, she joined Optical and Radio Communications Research Laboratories and in 1996, she joined Adaptive Communications Research Laboratories, Advanced Telecommunication Research International. Her work on the direction-of-arrival estimation based on MUSIC algorithm yielded an algorithm Smart MUSIC which shows the interpretation of eigenvalue analysis and the alternative algorithm to it without the eigenvalue analysis. She was awarded three patents from this work in 1999. She had an academic invitation related to this work at Kiruna Division, Swedish Institute of Space Physics, Sweden, in December 1996. In 1998, she joined Manchester Computing at the University of Manchester, Manchester, U.K. Since 2000, she has been a Lecturer in the School of Computer Science at the University of Manchester. Her current research interest resides in computational electromagnetics, especially, frequency dependent alternating direction implicit finite difference time domain method (FD-ADI-FDTD) for ultrawide-band systems.

In 2000, she received a Best Paper Award at the 8th International Conference on High Performance Computing and Networking Europe. She is a recipient of two grants, one of them is from EPSRC.

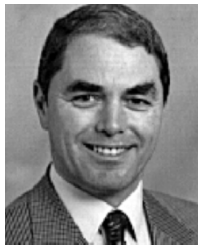

Stephen K. Barton (SM'92) received the B.Sc.(Eng.) degree in electronic and electrical engineering from University College London, London, U.K., in 1970 and the M.Sc. degree in telecommunications systems from the University of Essex, Essex, U.K., in 1974.

From 1970 to 1976, he was employed by Marconi Research Laboratories, principally on high speed fast acquisition modems for satellite TDMA. From 1976 to 1980, he was with Her Majesty's Government Communications Centre, working on GaAs FET oscillators and conformal antennas. From 1980 to 1985, he was with the Rutherford Appleton Laboratory, where he originated the Communications Engineering Research Satellite project. From 1985 to 1989, he was with Signal Processors Ltd., working on Adaptive TDMA modems and digital receivers generally. From 1989 to 1998, he was with the University of Bradford, from 1998 to 1999 he was with the University of Leeds, and since 1999 he has been with the University of Manchester, Manchester, U.K. His research interests include Wireless LANs, MAC and routing protocols, multicarrier modulation/demodulation, CDMA, channel equalization and near/far resistant detection algorithms. From 1993 to 1996, he was Chairman of Working Group 3: Broadband Systems, of the European Cooperation in Science and Technology programme: COST 231: Evolution of Land Mobile Radio (including personal) Communications. From 1997 to 2000, he was Chairman of Working Group 1: Radio System Aspects, of COST 259: Wireless Flexible Personalised Communications. Since 2001, he has been the U.K. National representative to COST 273: Toward Mobile Broadband Mutimedia Networks.

Prof. Barton is a Fellow of the Institution of Electrical Engineers (IEE).